RAL-85-020

Science and Engineering Research Council
Rutherford Appleton Laboratory
CHILTON, DIDCOT, OXON, OX11 0QX

RAL-85-020

The analysis of colliding-shock experiments

D K Bradley, J Hares, A Rankin and S J Rose

March 1985

RAL 84 020

The analysis of colliding-shock experiments

D.K.Bradley, J.Hares, A.Rankin,

Plasma Physics Department,

Blackett Laboratory,

Imperial College,

Prince Consort Road,

London, SW7 2BZ,

Great Britain.

and

S.J.Rose,

Rutherford Appleton Laboratory,

Chilton,

Didcot,

Oxfordshire, OX11 0QX,

Great Britain.

Abstract

X-ray radiographic and photoabsorption measurements are descibed of material which has been highly compressed and strongly heated by laser-driven colliding shocks. Theoretical work which attempts to interpret the data is also presented. The experimental data appears to favour one particular formulation of the continuum lowering.

1. Introduction

High-power lasers are unique in that they can produce material temperatures and densities which are more extreme than can otherwise be obtained in the laboratory. Apart from its intrinsic interest, the study of material under such conditions is of relevance to the study of stellar structure and inertial confinement fusion. In this paper, experiments are described in which time-resolved X-ray radiographic and photoabsorption measurements of compressed and heated material are made, together with theoretical work which attempts to interpret the data.

2. Experimental arrangement

The experiments involved two-sided irradiation of planar targets. Planar geometry is particularly amenable to diagnostic probing, allowing both streaked radiography and streaked photoabsorption measurements to be made.

The radiographic experimental arrangement is shown in figure 1. The targets are self-backlighting by means of a bismuth strip. The compression is followed by means of the X-ray shadow of the two buried bismuth tracer layers. The angle of view, θ, is a compromise between target absorption (lower for larger θ) and resolution (better for smaller θ). The angle chosen (30°) gave a backlighting cutoff energy of 2.5keV and a spatial resolution (with a 4μm pinhole in front of the streak camera) of approximately 8μm. Figure 2 shows a streaked radiograph from shot #11 14/12/83 (details of which are given in table 1) showing a compression of ≥ 6, the lower limit being set by resolution.

The second set of experiments involved photoabsorption spectroscopy. The region near the K-absorption edge was chosen for study because it lies at a suitable wavelength for both backlighter and detector. Chlorine was incorporated into the targets by replacing a central layer of N-parylene (C_8H_8) by C-parylene (C_8H_7Cl). A thin layer of bismuth was incorporated on one side of the targets which allowed them to be self-backlighting. To record the photoabsorption spectrum a germanium crystal spectrometer was used on the front of miniature re-entrant streak camera. The spectral resolution was approximately 2eV at the chlorine K-edge with a time resolution of about 150 psec. The backlighting continuum intensity was sufficient to record an absorption jump ratio of five. Figure 3 shows the experimental arrangement together with target details. Figure 4 shows a streak record from shot #13 21/12/83 (details of which are given in table

$$Z_i^* = 4\pi R_i^3 n(R_i)/3 \qquad (1)$$

where R_i is the ion-sphere radius of element i and n(r) is the Thomas-Fermi electron number density at radius r. The average charge on an ion in the mixture is

$$Z_{mix}^* = \sum_i f_i Z_i^* \qquad (2)$$

and the average ion-sphere radius is

$$R_{mix} = \left[\sum_i f_i R_i^3\right]^{1/3} \qquad (3)$$

where f_i is the fraction by number density of element i in the mixture.

The average strong-coupling parameters for the mixture are

$$\Gamma_{ii} = \frac{(Z_{mix}^* e)^2}{R_{mix} kT} \qquad (4)$$

and

$$\Gamma_{ee} = \frac{e^2}{r_{ee} kT} \qquad (5)$$

where r_{ee} is the free-electron analogue of the ion-sphere radius

$$r_{ee} = \frac{R_{mix}}{(Z^*_{mix})^{1/3}} \qquad (6)$$

The plasma parameters Z^*_{Cl}, Z^*_{mix}, Γ_{ii} and Γ_{ee} are shown for different temperatures and densities in figures 8 and 9.

(iii) K-edge shift calculations.

The shift in the energy of the chlorine K-edge in C-parylene is given by

$$\Delta E_K(\rho,T) = E_K(\rho,T) - E_K(\rho_0,T_0) \qquad (7)$$

where $E_K(\rho,T)$ is the energy of the chlorine photoabsorption K-edge at temperature T and density ρ, and where T_o and ρ_o are the normal temperature and density of C-parylene (2.6×10^{-5} eV and 1.29g/cc respectively). $E_K(\rho,T)$ is calculated as the sum of three terms:

$$E_K(\rho,T) = I_K(\rho,T) + \Delta E_{deg}(\rho,T) + \Delta E_{cl}(\rho,T) \qquad (8)$$

The first term (I_K) represents the K-shell ionization energy of a free chlorine ion averaged over the different chlorine ions found in the plasma. Degeneracy in the free electron system increases the photoabsorption edge energy and this is represented by the second term (ΔE_{deg}). The effect of the plasma neighbours is to reduce the photoabsorption edge energy and this change is represented by the third term (ΔE_{cl}).

(a) The calculation of I_K.

For integer Z^*_{Cl} , I_K is approximated as the K-shell ionization energy of the ground-state chlorine ion with the outer Z^*_{Cl} electrons removed. Calculations are required to obtain the ionization energies as experimental values are not available. Because electronic transitions from the K-shell are involved, relativistic effects must be included for accuracy and the multiconfiguration Dirac-Fock (MCDF) programs of Grant et al[2] and McKenzie et al[3] are used. Values of the ionization energy for different ground-state ions of chlorine calculated by these programs are given in table 2. Comparison of experimental K-shell ionization energies of noble gases with values calculated from the MCDF programs[4] suggest that the values in table 2 are accurate to within a few eV. For non-integer Z^*_{Cl} , I_K is obtained by linear interpolation between the values for integer Z^*_{Cl}.

(b) The calculation of ΔE_{deg} .

The effect of free electron degeneracy is to fill the low-energy states shifting the photoabsorption edge to higher energy. The probability, p, that a free electron state of energy ϵ is filled is given by

$$p = 1/(e^{(\epsilon-\mu)/kT}+1) \qquad (9)$$

where μ comes from the Thomas-Fermi calculations. For $\mu < 0$ (non-degenerate electrons), $p<1/2$, whilst for $\mu>0$ (degenerate electrons)

$$\begin{aligned} p &< 1/2 \quad \text{for} \quad \epsilon > \mu \\ p &= 1/2 \quad \text{for} \quad \epsilon = \mu \\ p &> 1/2 \quad \text{for} \quad \epsilon < \mu \end{aligned} \qquad (10)$$

showing that

$$\Delta E_{deg} = \begin{cases} \mu & \mu > 0 \\ 0 & \mu < 0 \end{cases} \qquad (11)$$

Values of μ at different temperatures and densities are shown in figure 10.

(c) Continuum lowering.

In this work three different models of continuum lowering have been considered.

Model 1 - Ion-sphere.

The ion-sphere model in its simplest form has a uniform distribution of free electrons which neutralise the ionic charge and neighbouring plasma particles do not penetrate inside the ion-sphere volume. Continuum lowering arises from a change in the energy of a bound electronic level by the interaction with the free electrons in the ion-sphere. Using first-order perturbation theory, the shift in energy is

$$\Delta\epsilon = \int d\tau(-e\psi^2)V \qquad (12)$$

where ψ is the wavefunction of the chlorine ion and V is the potential resulting from the free electrons. For Z^* free electrons in an ion-sphere of radius R, the potential is given by

$$V(r) = \frac{Z^* e}{2R}\left[\frac{r^2}{R^2} - 3\right] \qquad (13)$$

The difference in the perturbation between a chlorine ion (denoted i) and

the same ion after K-shell ionization (denoted f) is

$$\Delta E = \int -e\psi_f^2\left[\frac{Z^* e}{2R}\left(\frac{r^2}{R^2}-3\right)\right] d\tau - \int -e\psi_i^2\left[\frac{Z^* e}{2R}\left(\frac{r^2}{R^2}-3\right)\right] d\tau$$

$$= \frac{Z^* e^2}{2R}\left\{\left[\frac{\sum_k n_k^f \langle r_k^2\rangle^f - \sum_k n_k^i \langle r_k^2\rangle^i}{R^2}\right] - 3\right\} \qquad (14)$$

where n_k^i and n_k^f are the average-of-configuration occupation numbers of electron k in state i and f respectively for the chlorine ions of average ionization state Z^*. Denoting

$$\Delta r(Z^*)^2 = \sum_k n_k^f \langle r_k^2\rangle^f - \sum_k n_k^i \langle r_k^2\rangle^i \qquad (15)$$

then in this model the expression for the continuum lowering is

$$\Delta E_{cl} = \frac{Z_{cl}^* e^2}{2R_{cl}}\left[\frac{\Delta r(Z_{cl}^*)^2}{R_{cl}^2} - 3\right] \qquad (16)$$

Because Z_{Cl}^* is in general non-integer, the value of $\Delta r(Z_{Cl}^*)^2$ is obtained by linear interpolation from the values at integral Z_{Cl}^* (table 3).

Model 2 - Augmented ion-sphere.

The second model uses equation (16) with a correction for the interaction energy of the ionised electron with the plasma. The correction is evaluated assuming a uniform ionised electron density interacting with the plasma, described by an ion-sphere model of radius R_{mix} (equation 3),

ion charge Z^*_{mix} (equation 4) and with Z^*_{mix} uniformally distributed free electrons. The modified expression for the continuum lowering is then

$$\Delta E_{cl} = \frac{Z^*_{cl} e^2}{2R_{cl}}\left[\frac{\Delta r (Z^*_{cl})^2}{R^2_{cl}} - 3\right] - \frac{3Z^*_{mix}}{10R_{mix}} \qquad (17)$$

Model 3 - Neighbouring-ions model.

The modification of the potential experienced by an ionizing electron due to the presence of neighbouring ions allows a different description of the continuum lowering to that in an ion-sphere model. From figure 11 the value of the correction is given by

$$\Delta E_{cl} = -\left\{\frac{Z^*_{cl}+1}{r} + \frac{Z^*_{mix}}{2R_{mix}-r}\right\} e^2 \qquad (18)$$

evaluated at the turning point $\partial \Delta E_{cl} / \partial r = 0$.

Using these models estimates of the position of the chlorine K-edge in cold C-parylene at normal density ($E_K(\rho=\rho_o, T=T_o)$ can be made. Continuum lowering models 1,2 and 3 predict 2.853,2.849 and 2.835 keV respectively, in comparison with an experimental value 2.826 keV. Figures 12,13 and 14 show the values of the shift in position of the K-edge with increasing density and temperature. Neither of the ion-sphere models produce a red-shift under the peak temperature and density conditions predicted to occur in the photoabsorption experiment, whereas model 3 predicts a red-shift of approximately 15 eV in fairly good agreement with the 10 eV observed experimentally.

One of the major uncertainties in the modelling of the photoabsorption experiment is the Thomas-Fermi calculation of the

ionization balance. Using the expression for Z_i^* given in equation (1), finite ionization is predicted at zero temperature and normal density. The Thomas-Fermi model does not include chemical effects and calculations have been performed which adjust the Thomas-Fermi ionization to predict at $T=T_o$ and $\rho=\rho_o$, the existence of Cl^- ions in C-parylene:

$$\left.\begin{aligned} Z^*_{Cl} &\to -1 \\ Z^*_{C} &\to +1/8 \\ Z^*_{H} &\to 0 \end{aligned}\right\} T\to 0 \quad \text{and} \quad \left.\begin{aligned} Z^*_{Cl} &\to 17 \\ Z^*_{C} &\to 6 \\ Z^*_{H} &\to 1 \end{aligned}\right\} T\to\infty$$

It is believed that this probably gives a more realistic description of the state of ionization than using equation (1). However, although this improves the predicted value of $E_K(\rho=\rho_o, T=T_o)$ (2.819 keV from models 1,2 and 3), model 3 is still in substantially better agreement with experiment than models 1 or 2 (at a temperature of 15 eV and a compression of 6, models 1,2 and 3 predict shifts of +19.2, +11.8 and -11.7 eV respectively).

A calculation of the observed width of the K-edge has not been attempted. Several mechanisms will contribute , including non-uniformities of temperature and density, and electron degeneracy.

4. Conclusions.

It has been shown that two-sided laser irradiation of a planar target can prduce a plasma which is calculated to be both degenerate and strongly-coupled, in a geometry that is amenable to probing. Streaked X-ray radiography gives information on the density which is consistent with hydrodynamic simulations. Streaked X-ray photoabsorption spectra of the plasma near the chlorine K-edge have also been obtained. Ion-sphere models of continuum-lowering do not give good agreement with experiment, whereas this is achieved using a neighbouring-ions model. It appears therefore, on the basis of the calculations reported here, that the experimental data favours one particular formulation of the continuum lowering.

There are, however, many uncertainties in the modelling of the experiment, particularly in the neglect of the bismuth backlighter in the hydrodynamic simulations. The inclusion of the bismuth has not been attempted because the radiation transport models are unreliable both in their ability to calculate radiation transport in high-Z materials and also in handling the difficult geometry in the radiographic shot.

Because of the uncertainties, the conclusions must remain tentative. However it is proposed that in future experiments the backlighter is removed from the target, replacing it by a point source. It is hoped that in this way radiative preheating will be greatly reduced.

Table 1. Radiographic and Photoabsorption Shot Details.

Shot type	Radiographic	Photoabsorption
Shot number	#11 14/12/83	#13 21/12/83
North beam energy (J)	29.6	31
South beam energy (J)	27.6	29
Spot diameter (μm)	110	150
Pulse length (nsec)	1.5	1.5
Average intensity (W/cm^2).	2.01×10^{14}	1.13×10^{14}
Target details	0.35μm bismuth strip/ 7μm N-parylene/ 48μm mylar/ 7μm N-parylene. (0.1μm vertical bar on each side of mylar region).	0.35μm bismuth/ 18μm N-parylene/ 21μm C-parylene/ 18μm N-parylene.

Table 2. Chlorine K-shell ionization energies.+

Ionization state	Ground configuration	K-shell ionization energy (keV)
0	$1s^2\,2s^2\,2p^6\,3s^2\,3p^5$	2.8312
1	$1s^2\,2s^2\,2p^6\,3s^2\,3p^4$	2.8461
2	$1s^2\,2s^2\,2p^6\,3s^2\,3p^3$	2.8633
3	$1s^2\,2s^2\,2p^6\,3s^2\,3p^2$	2.8827
4	$1s^2\,2s^2\,2p^6\,3s^2\,3p$	2.9040
5	$1s^2\,2s^2\,2p^6\,3s^2$	2.9276
6	$1s^2\,2s^2\,2p^6\,3s$	2.9537
7*	$1s^2\,2s^2\,2p^6$	2.9798

+Calculated as the difference in energy between two separately optimised average-of-configuration Dirac-Fock calculations, including the dynamic part of the interelectron interaction and quantum-electrodynamic effects.

*The K-shell ionization energy is calculated for every subsequent ion stage by increasing the value by 15eV.

Table 3. Values of Δr^2 (a.u.) for chlorine.†

Ionization state	Ground configuration	$\Delta r(Z^*)^2$
0	$1s^2\ 2s^2\ 2p^6\ 3s^2\ 3p^5$	7.2642
1	$1s^2\ 2s^2\ 2p^6\ 3s^2\ 3p^4$	4.7947
2	$1s^2\ 2s^2\ 2p^6\ 3s^2\ 3p^3$	3.2546
3	$1s^2\ 2s^2\ 2p^6\ 3s^2\ 3p^2$	2.1937
4	$1s^2\ 2s^2\ 2p^6\ 3s^2\ 3p$	1.4213
5‡	$1s^2\ 2s^2\ 2p^6\ 3s^2$	0.8384

† Calculated from two separately optimised Dirac-Fock calculations.

‡ The value of Δr^2 for higher ionization states is taken as zero.

References.

1. Christiansen J.P., Ashby D.E.T.F. and Roberts K.V., Computer Physics Communications 7,271 (1974).

2. Grant I.P., McKenzie B.J., Norrington P.H., Mayers D.F. and Pyper N.C., Computer Physics Communications 21, 207 (1980).

3. McKenzie B.J., Grant I.P., Norrington P.H., Computer Physics Communications 21, 233 (1980).

4. Beatham N., Grant I.P., McKenzie B.J. and Rose S.J., Physica Scripta 21, 423 (1980).

Figure captions.

Figure 1. Schematic plan of radiographic experiment.

Figure 2. Colour enhanced streak record of radiographic shot #11 14/12/83.

Figure 3. Schamatic plan of photoabsorption experiment.

Figure 4. Colour enhanced streak record of photoabsorption shot #13 21/12/83.

Figure 5. Calculated average compression of mylar between tracer strips in radiographic shot #11 14/12/83.

Figure 6. Calculated average temperature and compression of C-parylene in photoabsorption shot #13 21/12/83.

Figure 7. Calculated temperature and compression through C-parylene in photoabsorption target (shot #13 21/12/83) at 1.7 nsec.

Figure 8. Ionization states in C-parylene.

Figure 9. Strong-coupling parameters in C-parylene.

Figure 10. Degeneracy parameters in C-parylene.

Figure 11. Contributions to the potential energy in continuum lowering model 3.

Figure 12. K-edge shift calculated using continuum-lowering model 1.

Figure 13. K-edge shift calculated using continuum-lowering model 2.

Figure 14. K-edge shift calculated using continuum-lowering model 3.

Figure 1.

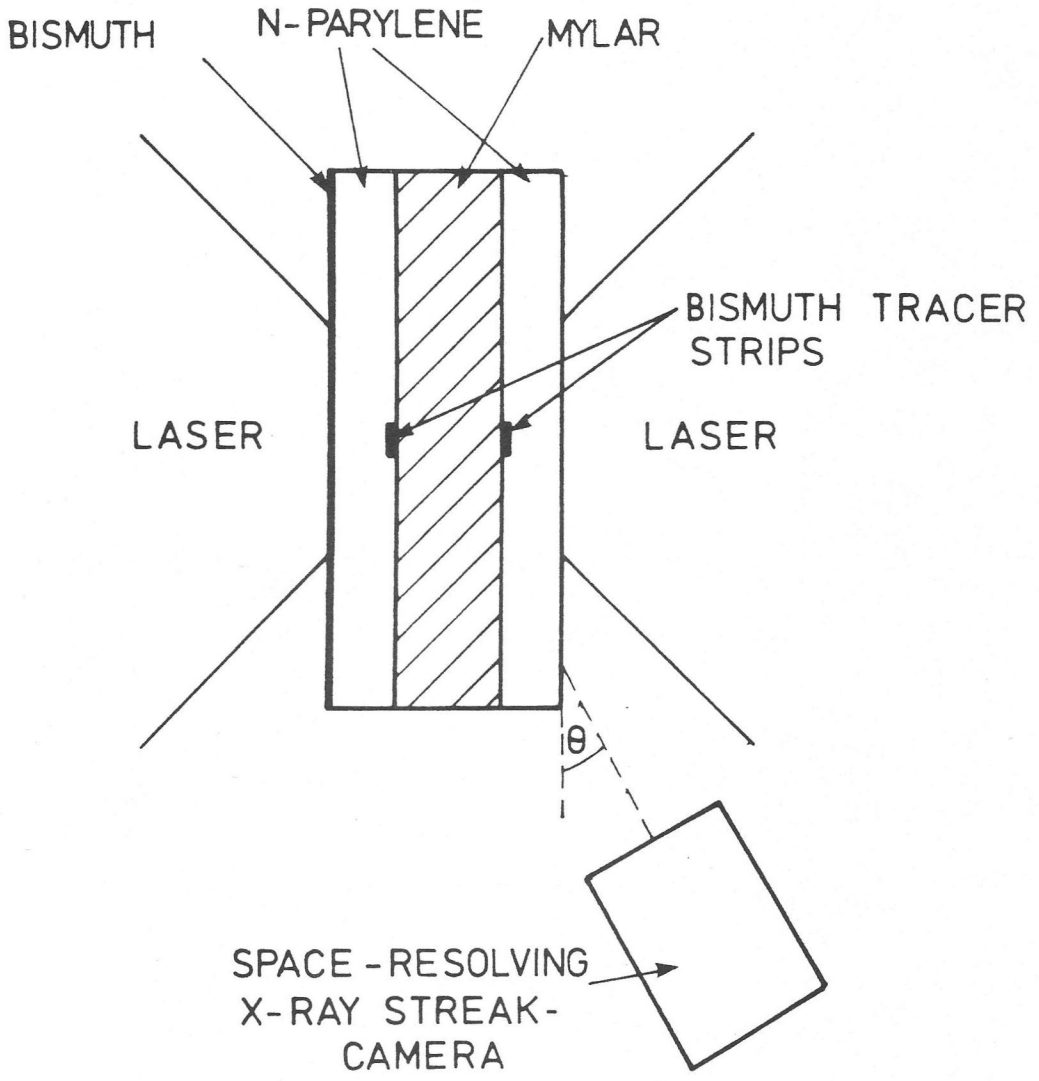
BISMUTH
N-PARYLENE
MYLAR
BISMUTH TRACER STRIPS
LASER
LASER
θ
SPACE-RESOLVING X-RAY STREAK-CAMERA

Figure 2.

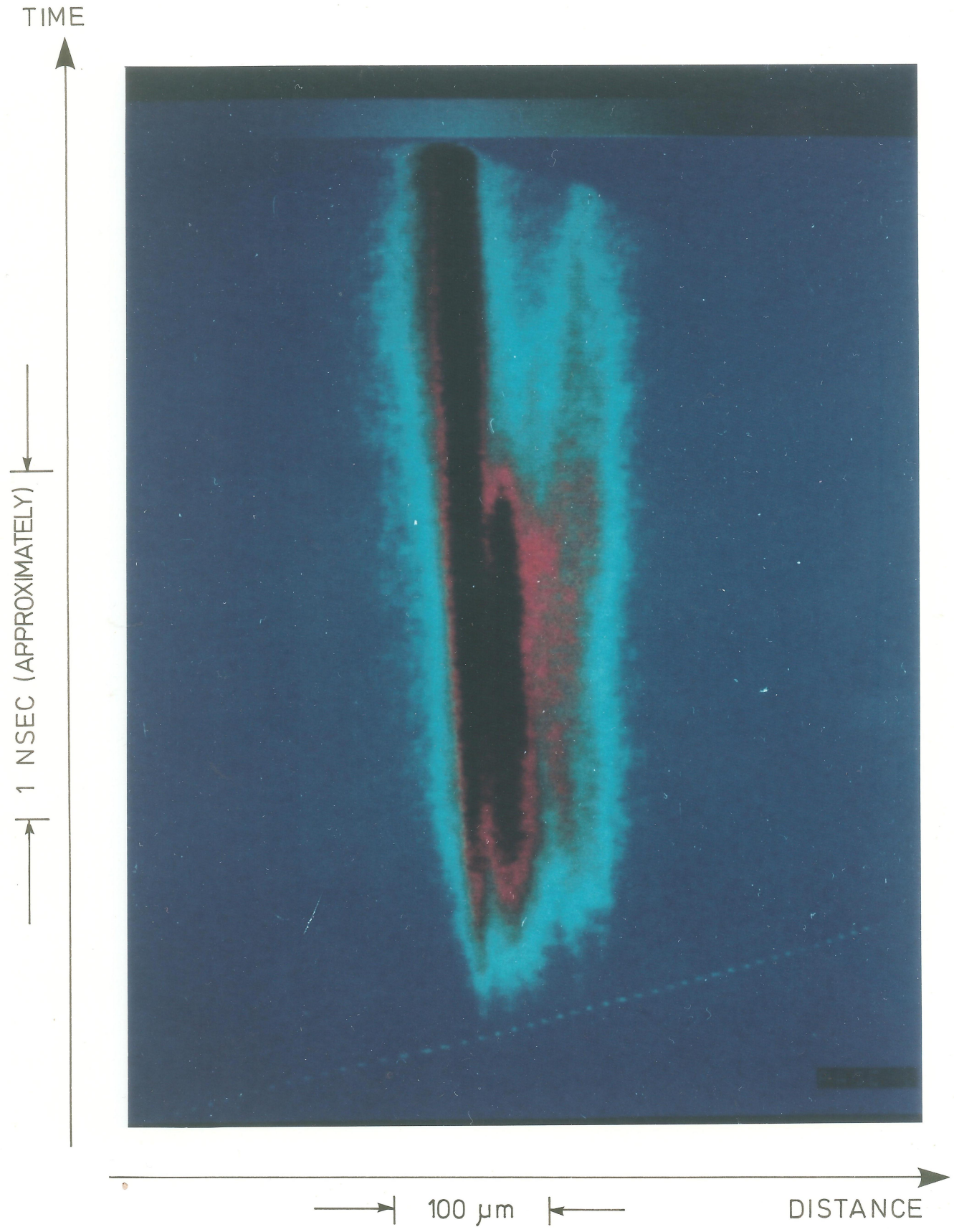

Figure 3.

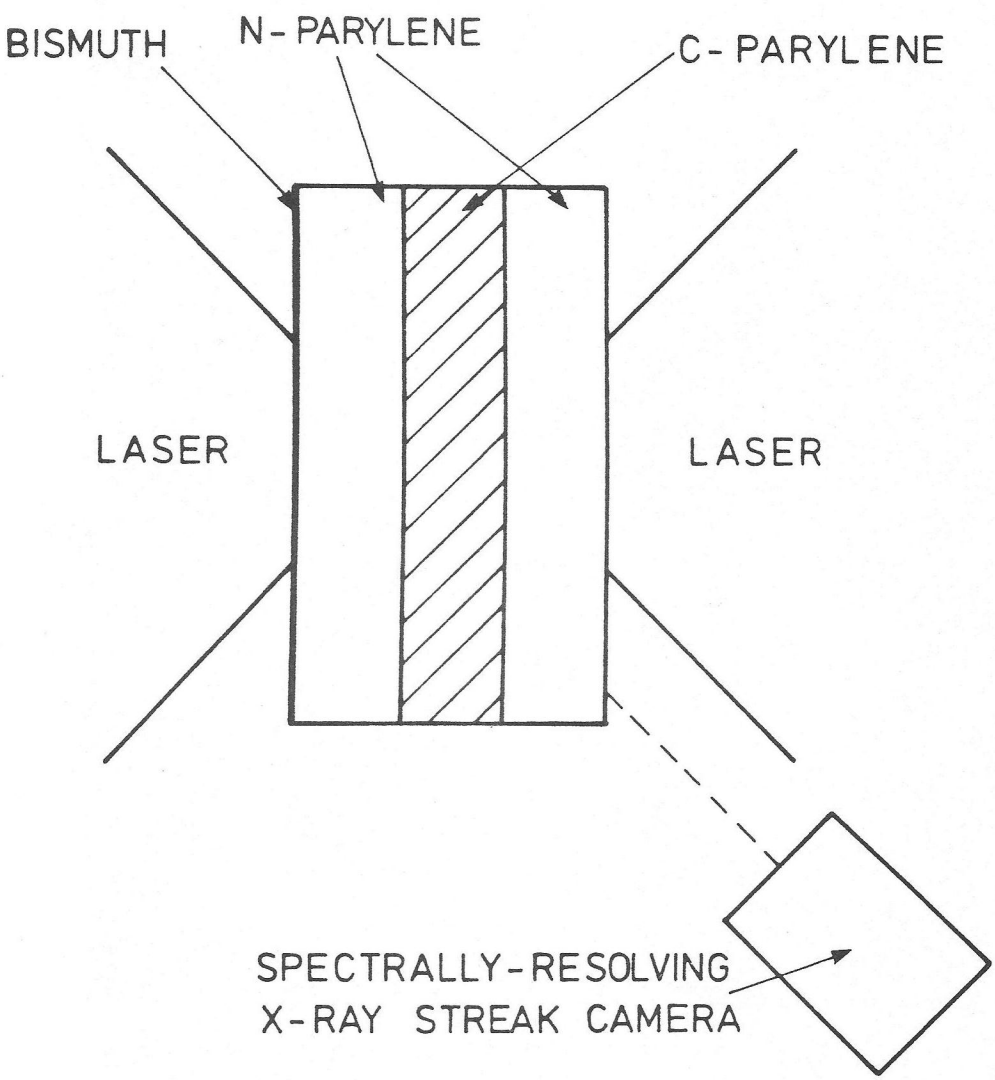
BISMUTH
N-PARYLENE
C-PARYLENE
LASER
LASER
SPECTRALLY-RESOLVING
X-RAY STREAK CAMERA

Figure 4.

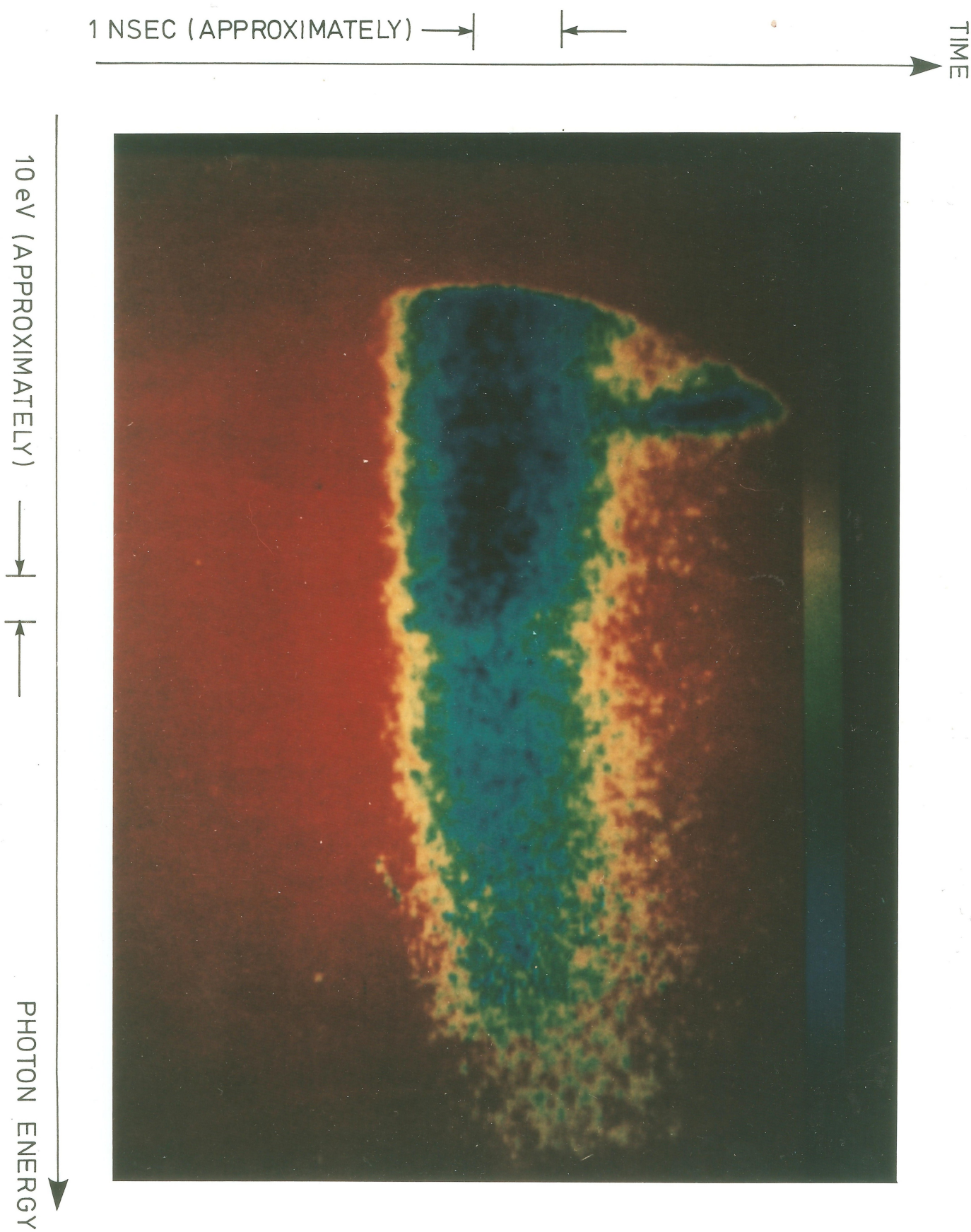
1 NSEC (APPROXIMATELY)
TIME
10 eV (APPROXIMATELY)
PHOTON ENERGY

Figure 5.

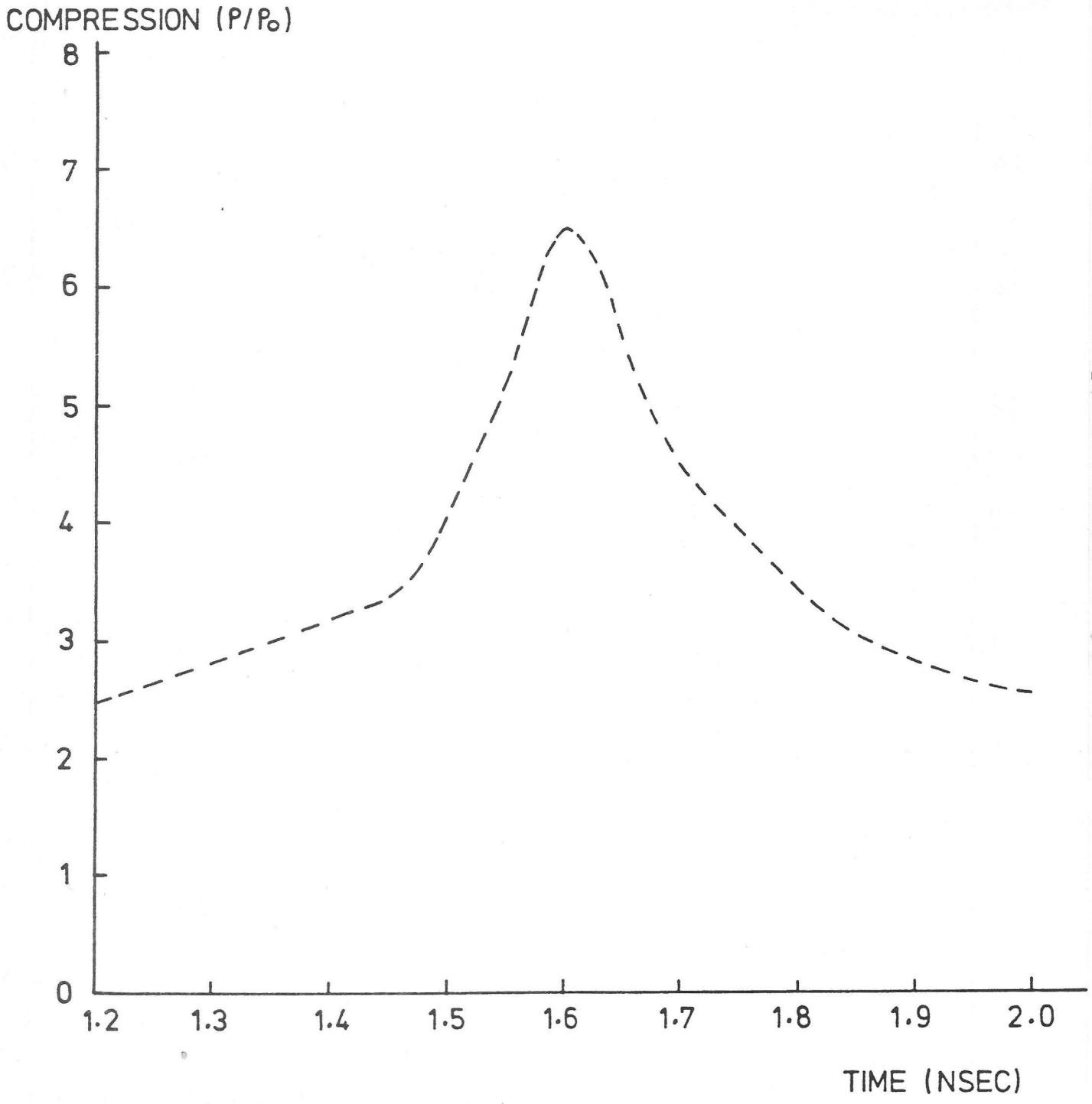

Figure 6.

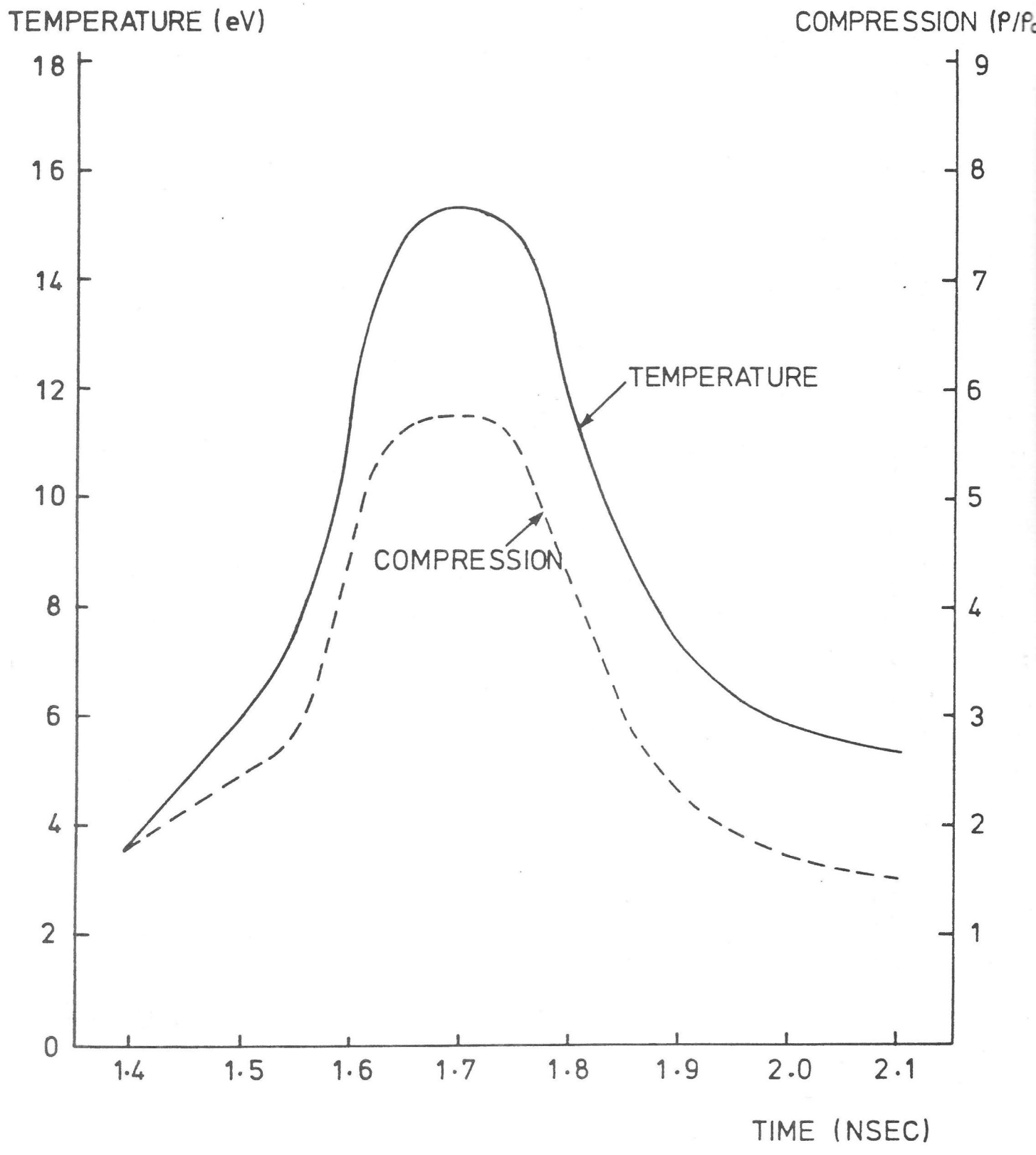
TEMPERATURE (eV)
COMPRESSION (P/P
18
16
14
12
10
8
6
4
2
0
9
8
7
6
5
4
3
2
1
TEMPERATURE
COMPRESSION
1·4
1·5
1·6
1·7
1·8
1·9
2·0
2·1
TIME (NSEC)

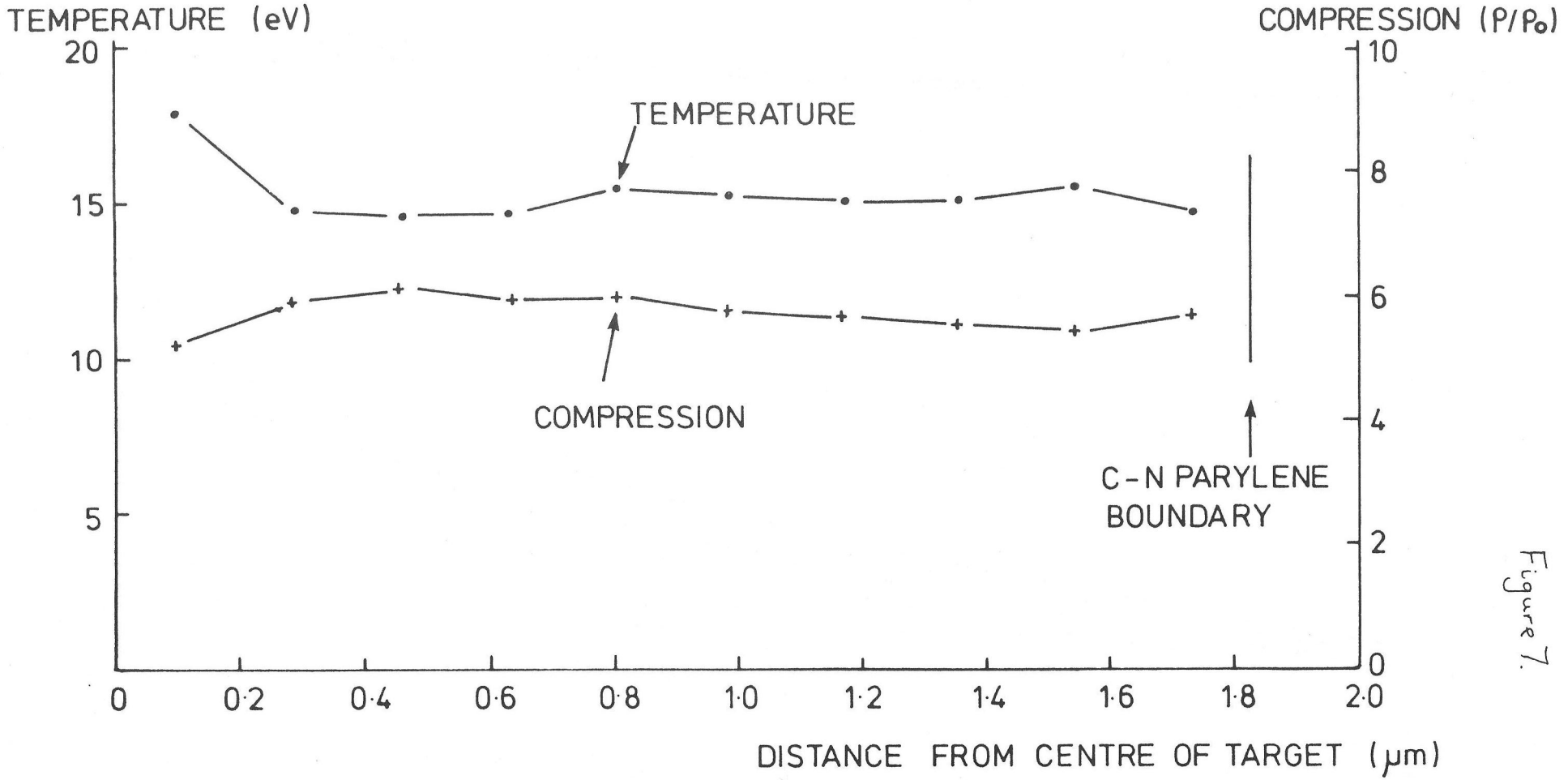
TEMPERATURE (eV)
COMPRESSION (P/P₀)
20
15
10
5
10
8
6
4
2
0
TEMPERATURE
COMPRESSION
C-N PARYLENE
BOUNDARY
0
0·2
0·4
0·6
0·8
1·0
1·2
1·4
1·6
1·8
2·0
DISTANCE FROM CENTRE OF TARGET (μm)

Figure 7.

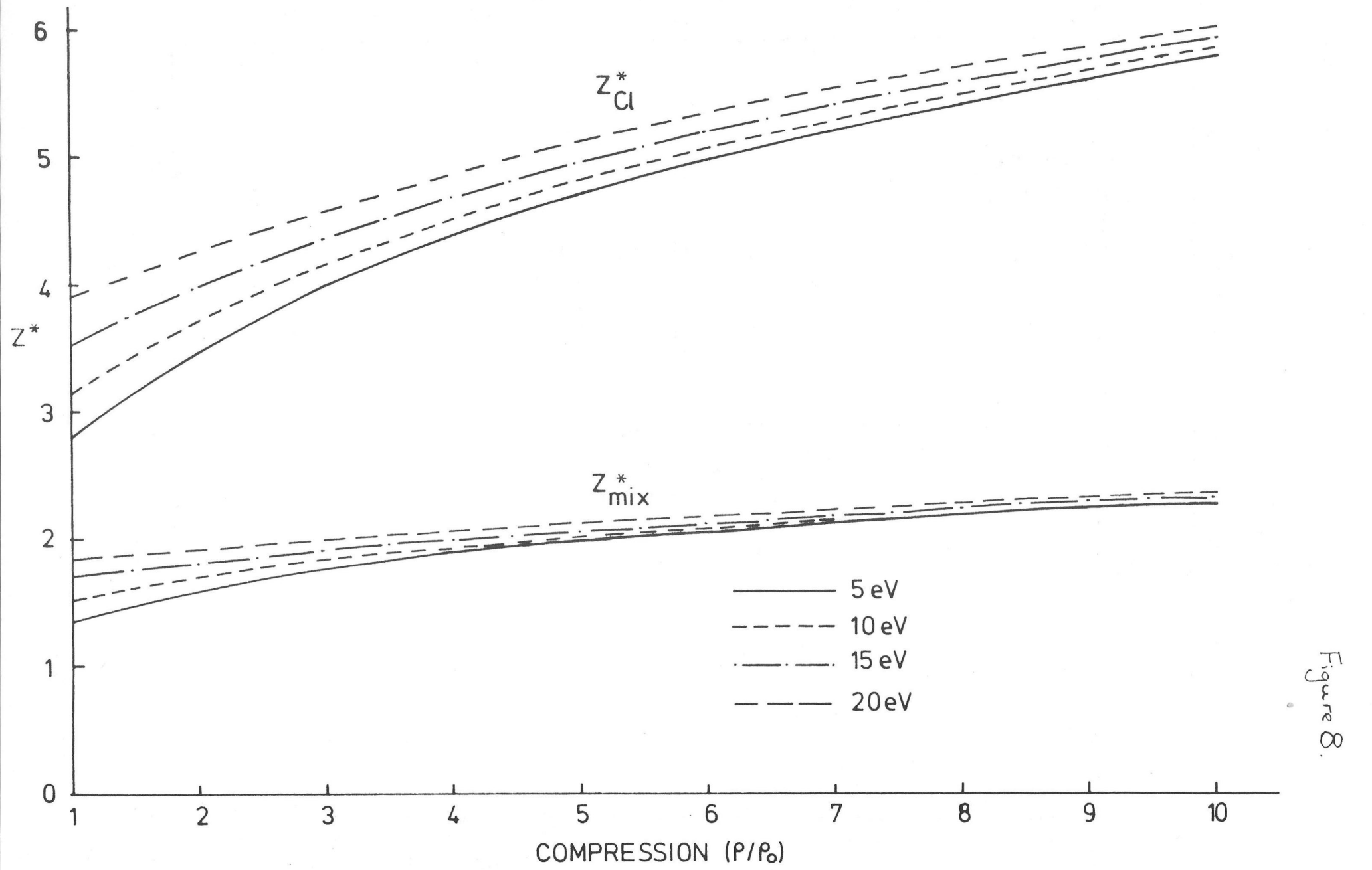
6
5
4
3
2
1
0
Z*
Z^*_{Cl}
Z^*_{mix}
5 eV
10 eV
15 eV
20 eV
1
2
3
4
5
6
7
8
9
10
COMPRESSION (P/P₀)

Figure 8.

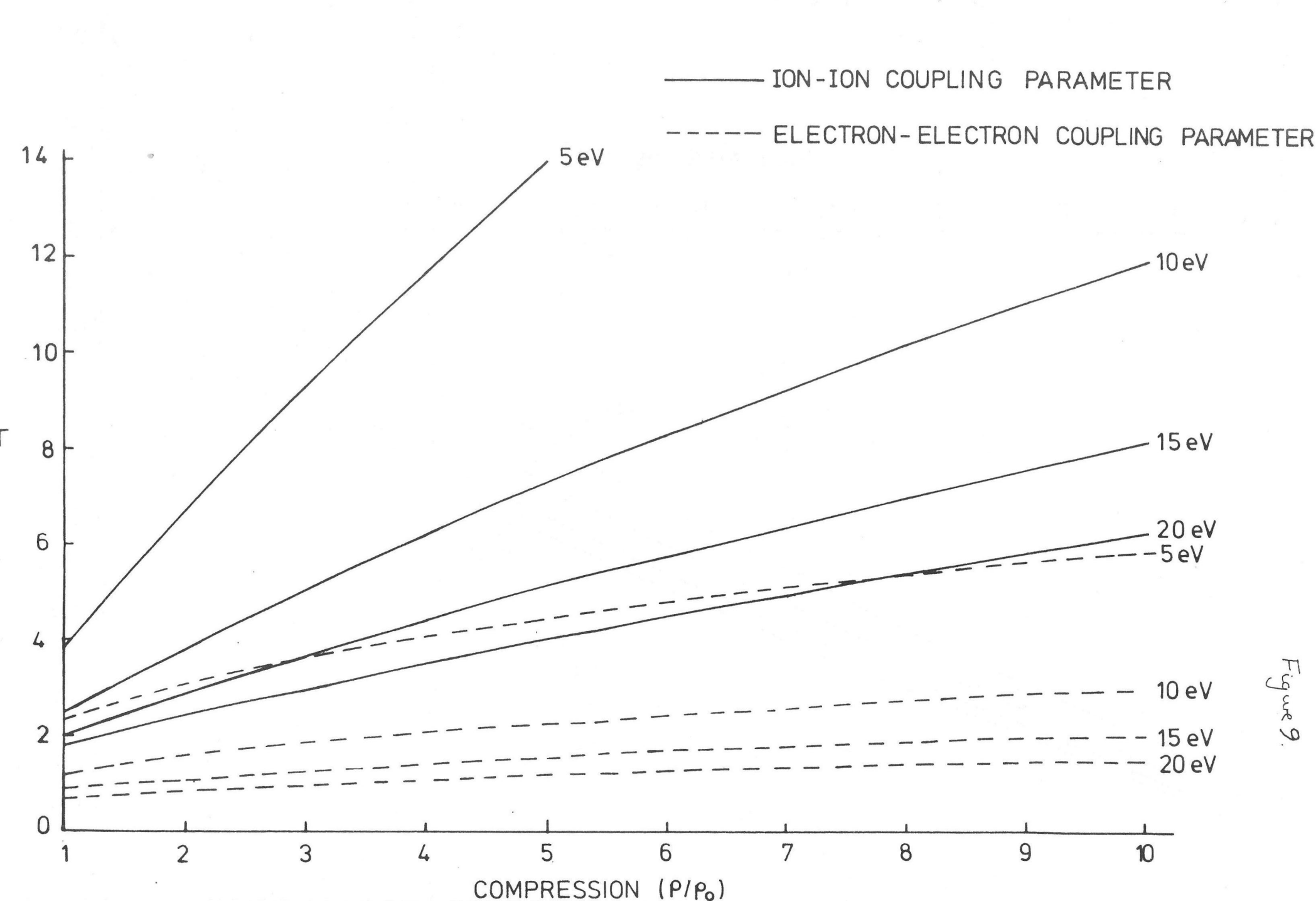
ION-ION COUPLING PARAMETER
ELECTRON-ELECTRON COUPLING PARAMETER
5 eV
10 eV
15 eV
20 eV
5 eV
10 eV
15 eV
20 eV
14
12
10
8
6
4
2
0
1
2
3
4
5
6
7
8
9
10
COMPRESSION (P/P₀)

Figure 9.

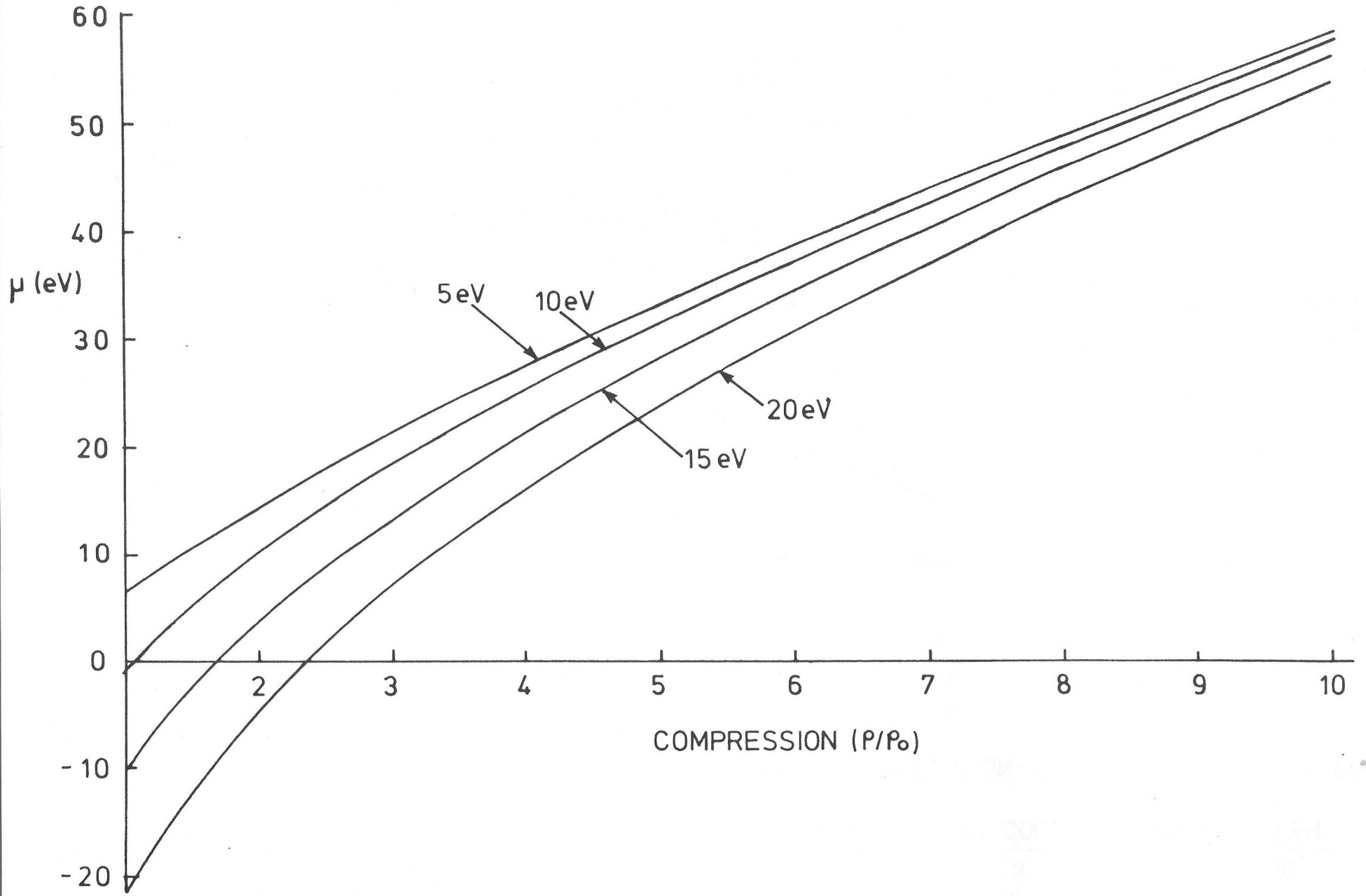
60
50
40
μ (eV)
30
20
10
0
-10
-20
5eV
10eV
15eV
20eV
2
3
4
5
6
7
8
9
10
COMPRESSION (P/Po)

Figure 10.

Figure 11.

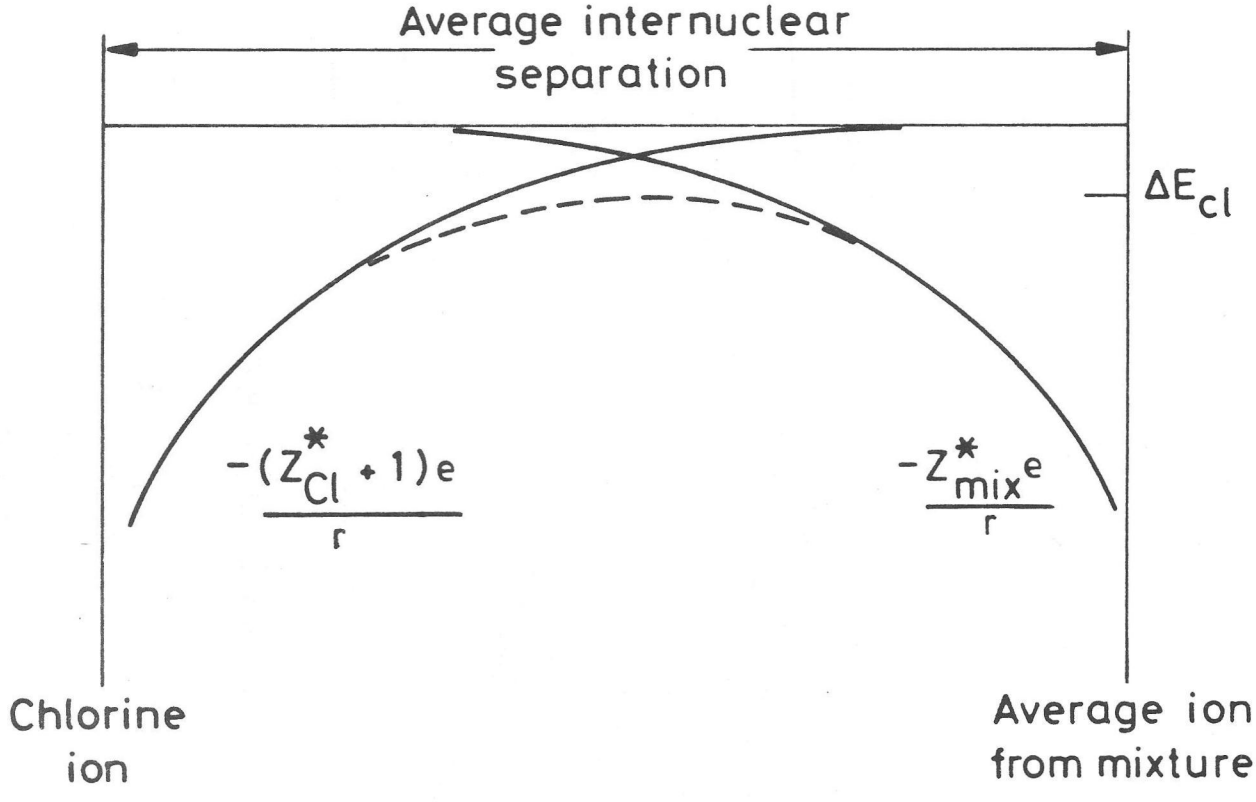
Average internuclear separation
ΔE_{Cl}
$-\frac{(Z^*_{Cl}+1)e}{r}$
$-\frac{Z^*_{mix}e}{r}$
Chlorine ion
Average ion from mixture

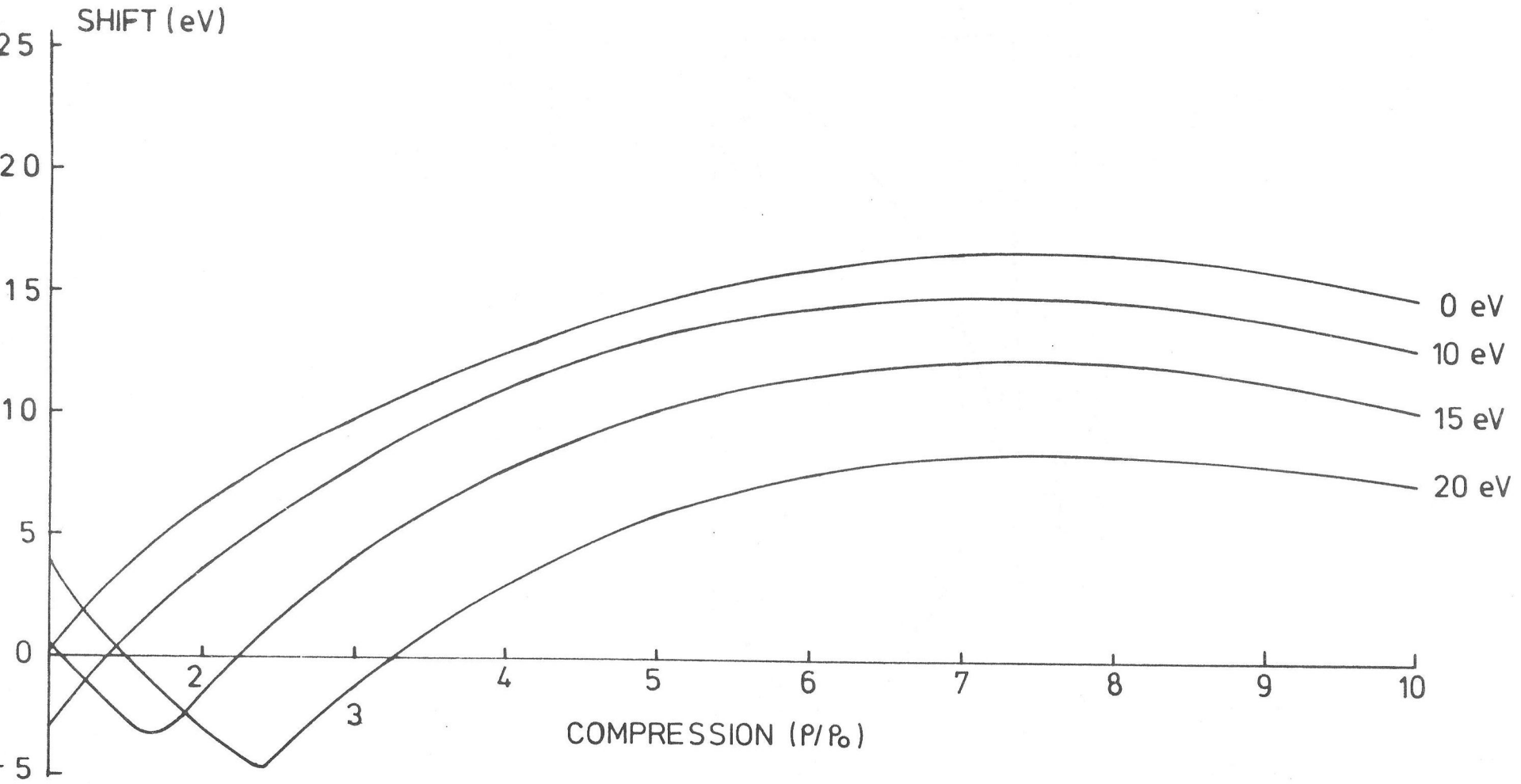
SHIFT (eV)
25
20
15
10
5
0
-5
0 eV
10 eV
15 eV
20 eV
2
3
4
5
6
7
8
9
10
COMPRESSION (P/P₀)

Figure 12.

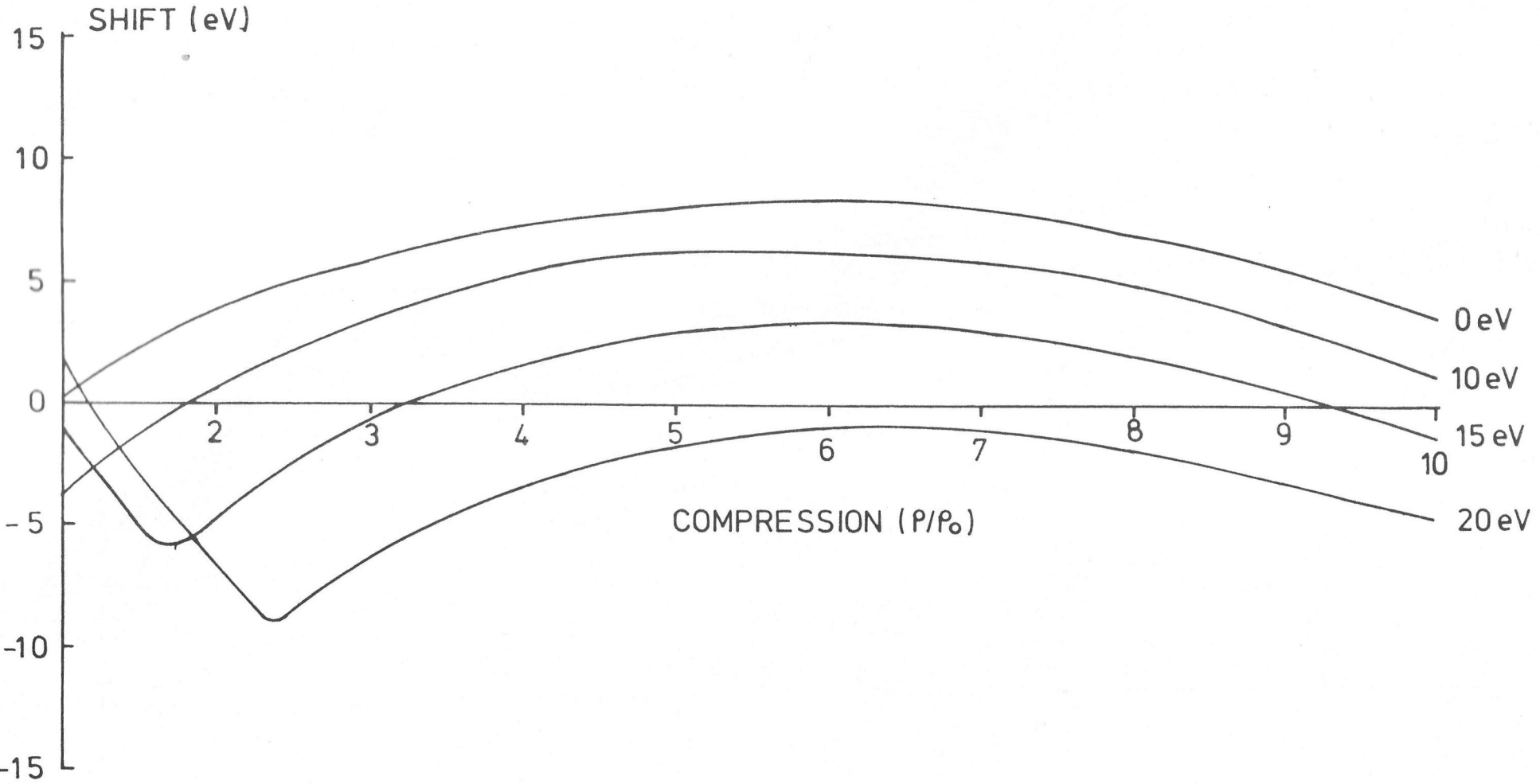
SHIFT (eV)
15
10
5
0
-5
-10
-15
2
3
4
5
6
7
8
9
10
COMPRESSION (P/P₀)
0 eV
10 eV
15 eV
20 eV

Figure 13.

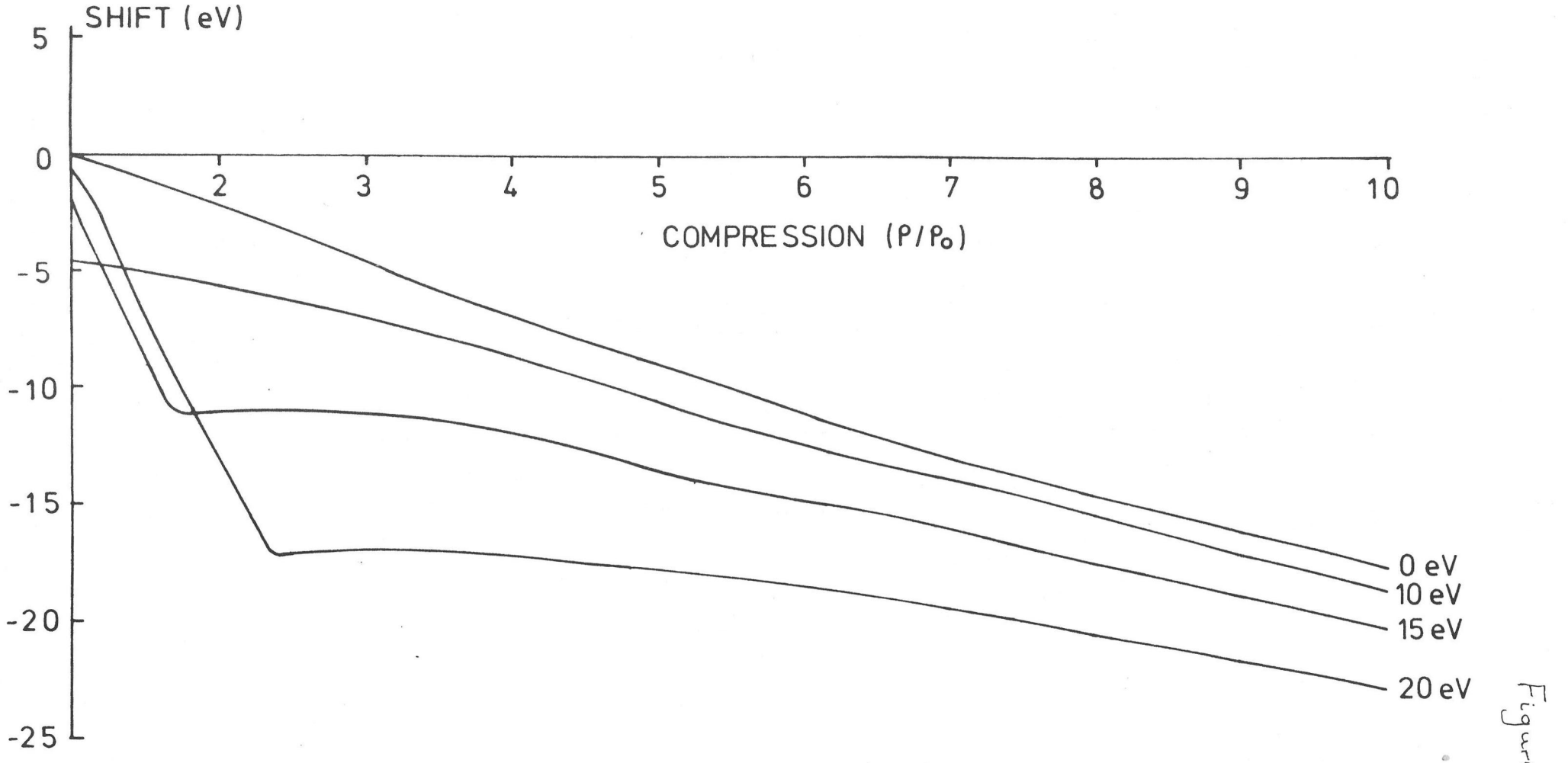
SHIFT (eV)
5
0
-5
-10
-15
-20
-25
2
3
4
5
6
7
8
9
10
COMPRESSION (P/P₀)
0 eV
10 eV
15 eV
20 eV

Figure 14.